Structural Properties of L-X-L-Met-L-Ala Phosphonate Tripeptides: A Combined FT-IR, FT-RS, and SERS Spectroscopy Studies and DFT Calculations

Edyta Podstawka,*,† Paweł Kafarski,‡ and Leonard M. Proniewicz§

Laser Raman Laboratory, Regional Laboratory of Physicochemical Analysis and Structural Research, and Chemical Physics Division, Faculty of Chemistry, Jagiellonian University, ul. Ingardena 3, 30-060 Krakow, Poland, and Department of Bioorganic Chemistry, Faculty of Chemistry, Wroclaw Technical University, ul. Wybrzeże Wyspiańskiego 27, 50-370 Wroclaw, Poland

Received: April 27, 2008; Revised Manuscript Received: August 31, 2008

FT-IR and FT-RS spectra of three phosphonate tripeptides containing P-terminal L-Met-L-Ala [L-Gly-L-Met-L-Ala-PO_3H_2 (**GMA**), L-Leu-L-Met-L-Ala-PO_3H_2 (**LMA**), and L-Phe-L-Met-L-Ala-PO_3H_2 (**PMA**)] were recorded and analyzed. Vibrational wavenumbers and intensities were calculated by density functional theory (DFT) at the B3LYP/6-311++G** level of theory and compared to these molecules in solid form. On the basis of this comparison, conclusions were drawn about the molecular structures. At the same time, the experimental data served as a test for the computational results. SERS spectra were recorded in a silver colloidal dispersion. Silver colloidal dispersions prepared by simple borohydride reduction of silver nitrate were used as substrates. A comparison is made between the SERS spectra and the spectra of the solid sample. Also, the capability of SERS for spectral fingerprinting of analytes with close structural properties using easily prepared substrates and relatively simple instrumentation is illustrated. By careful analysis, we obtained information on the orientation of these tripeptides and specific-competitive interactions of their functional groups with the silver surface. For example, all molecules are thought to adsorb on a silver surface via a P═O bond and a sulfur atom. In addition, the amide bond of **GMA** assists in the adsorption process, adopting a tilted orientation on the surface, with the N−H unit being closer to the surface than the C═O moiety. Conversely, the C═O unit of the **LMA** −CONH− bond lies closer to the silver surface than the N−H moiety. The $-CH_3$ group and P−O bond of **LMA** additionally interact with the silver surface, whereas for **PMA** the L-Phe lies almost flat on the colloidal silver surface.

Introduction

Peptides containing a C-terminal phosphonic acid analogue of alanine are among the most effective antibacterial agents.[1−3] Among them, tripeptides such as **GMA** (L-Gly-L-Met-L-Ala-PO_3H_2), **LMA** (L-Leu-L-Met-L-Ala-PO_3H_2), and **PMA** (L-Phe-L-Met-L-Ala-PO_3H_2) were synthesized and studied for their toxicity toward chosen strains of bacteria, and a relationship between this activity and the active transport of these tripeptides through bacterial cell walls was determined.[4,5]

Vibrational spectroscopy is widely used to predict the molecular structures of peptides.[6−8] Such studies have benefited from the advent of techniques such as Fourier transform infrared absorption spectroscopy (FT-IR), Fourier transform Raman spectroscopy (FT-RS), and surface-enhanced Raman scattering (SERS). The use of the Fourier transform technique, with the 1064-nm excitation wavelength, allows spectral details to be observed for molecules for which fluorescence and initiation of photoreactions are problems frequently encountered with excitation wavelength in the visible region of the electromagnetic radiation (normal Raman spectroscopy).[9] On the other hand, applications of SERS to the examination of molecular phenomena at metal−solution interfaces have become common in the last decades as an analytical technique for trace analysis and molecular characterization.[10−12] The SERS is notably the most widespread in situ technique for molecule recognition (biosensors creating), for the fundamental understanding of interfacial phenomena, and for a wide variety of technological applications, including microarrays, (bio)sensors, catalysis, and biocompatible coating. In the area of peptide screening, it is the first and crucial step for the functional and structural understanding of the activity of many hormones, host-defense peptides and lipopeptides, and toxins; for clarification of the principles that govern molecular recognition between membrane-spanning polypeptides and binding/association at the membrane interface; and for the formation mechanism of hard tissues such as bone and teeth or in biomineralization.[13−17] In this respect, various chemistry- and biology-based methods have been developed utilizing biotin−streptavidin interaction, antigen−antibody interaction, and protein−ligand (or protein−protein) interaction.[18−20]

From an analytical point of view, the most outstanding characteristic of SERS is that it provides a spectral fingerprint capability at the trace concentration level. This property arises due to the combination of the strong dependence of vibrational spectroscopy on structure and the enhancement of the Raman cross section of molecules on rough metallic surfaces.

However, assignments based upon empirical observations of structure−spectrum correlations sometimes can be misleading.[21] A better understanding of the relationship between the structure of peptides and their vibrational spectra is an aid in the interpretation of the complex data. The calculations by density functional theory (DFT), while perhaps restricted in scope, have an important role here. Without these studies, extension of such

* Corresponding author. Phone: +48-12-663-2255. Fax: +48-12-634-0515. E-mail: podstawk@chemia.uj.edu.pl.

† Laser Raman Laboratory, Regional Laboratory of Physicochemical Analysis and Structural Research, Jagiellonian University.

‡ Wroclaw Technical University.

§ Chemical Physics Division, Faculty of Chemistry, Jagiellonian University.

10.1021/jp803674q CCC: $40.75
Published on Web 10/23/2008

calculations to larger systems would be qualitative at best. Indeed, this is one of the reasons that many systems are studied by both theoretical and experimental methods.[22−27] A recent study employed the DFT method, using the hybrid functional B3LYP with the 6-311++G** basis set, to characterize **GMA**, **LMA**, and **PMA**. The results hinted strongly at the possibility of obtaining detailed structural parameters from the FT-RS and FT-IR spectra. This shows that, in agreement with conformational studies of tripeptides[28,29] (and larger molecules), vibrational calculations can yield valuable information. Hence, in the present paper we calculated the vibrational spectra of the aforementioned molecules. The calculated spectra for the zwitterionic species were compared to the experimental FT-IR and FT-RS spectra.

In the present paper, the SERS analysis of **GMA**, **LMA**, and **PMA** is reported for the first time. The aim of this part of the study was to explore the effects of amino acid substitution on the molecular orientation and interaction of these tripeptides with a solid surface, especially in terms of the presence of a sulfur atom in their structure. This is crucially important for a better understanding of the mechanisms of interaction between these biological molecules and their surrounding medium in terms of their substrate−receptor mechanism.

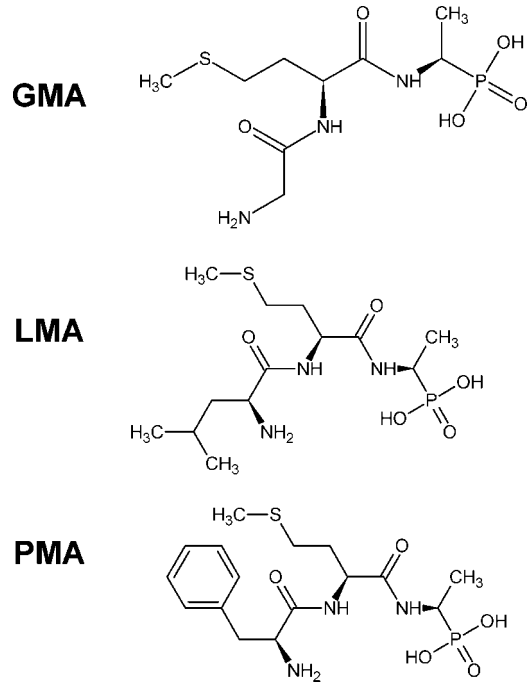

Figure 1. Molecular structures of L-Gly-L-Met-L-Ala-PO_3H_2 (**GMA**), L-Leu-L-Met-L-Ala-PO_3H_2 (**LMA**), and L-Phe-L-Met-L-Ala-PO_3H_2 (**PMA**).

Experimental Section

Peptide Synthesis. The following phosphonate tripeptides containing P-terminal L-Met-L-Ala-PO_3H_2 were synthesized according to a previously described procedure:[30] L-Gly-L-Met-L-Ala-PO_3H_2 (**GMA**), L-Leu-L-Met-L-Ala-PO_3H_2 (**LMA**), and L-Phe-L-Met-L-Ala-PO_3H_2 (**PMA**). The purity and chemical structures of the peptides were confirmed by their ^1H,^{31}P, and ^{13}C NMR spectra (Bruker Avance DRX 300 MHz spectrometer) and electrospray mass spectrometry (MALDI-TOF).

FT-RS Measurements. FT-RS measurements were performed for samples placed in a glass capillary tube. FT-RS spectra were recorded on a Bio-Rad step-scan spectrometer (model FTS 6000) combined with a Bio-Rad Raman accessory (model FTS 40) and a liquid nitrogen-cooled germanium detector. Typically, 1000 scans were collected with a resolution of 4 cm^{-1}. Excitation at 1064 nm was carried out using a Spectra-Physics continuous-wave Nd^{3+}:YAG laser (model Topaz T10-106c).

FT-IR Measurements. Thin palettes containing 1 mg of each tripeptide dispersed in 200 mg of KBr were used for FT-IR measurements. The spectra were recorded at room temperature as an average of 30 scans using a Bruker infrared spectrometer (model EQUINOX 55) equipped with a Nernst rod as the excitation source and a DT-GS detector in the 400−4000 cm^{-1} range with a spectral resolution of 4 cm^{-1}.

Computational Methods. All molecules studied in this work belong to the C_1 point symmetry group. Optimized structures, as well as their vibrational wavenumbers and intensities (absorbance and Raman intensity), were calculated by means of the Gaussian 03 suite of programs[31] using density functional theory (DFT) with the Becke three-parameter hybrid method and the Lee−Yang−Parr correlation functional (B3LYP)[32,33] using the 6-31++G** basis set. Such a procedure is commonly employed in calculations for similar compounds and gives reliable results.[22−26] During optimization, no imaginary wavenumbers were obtained, showing that the calculated structures correspond to energy minima on the potential energy surface for nuclear motion. The GaussSum 0.8 freeware program was utilized for checking outputs and generating theoretical spectra.[34] PEDs of normal modes in terms of natural internal coordinates were obtained with the GAR2PED freeware program.[35] To better reproduce the experimental spectra, we scaled all theoretical spectra with a uniform, empirical scaling factor of 0.975. Since the experimental measurements were performed on powder samples, we had to find a method for simulating the crystal environment (hydrogen bonds and incorporated water molecules) in our calculations. We applied the PCM (polarizable continuum model) as a first-order approximation of the crystal surroundings for the phosphonate tripeptides in this study. Despite its shortcomings, this approximation was sufficient to make our results comparable to the experimental spectra and effectively aided band assignments in the experimental spectra.

SERS Measurements. $AgNO_3$ and $NaBH_4$ were purchased from Sigma-Aldrich Co. (Poznan, Poland) and used without further purification. Three batches of colloidal silver solution were prepared according to the standard procedure.[36] Briefly, 8.5 mg of $AgNO_3$ dissolved in 50 mL of deionized water at 4 °C was added dropwise to 150 mL of 1 mM $NaBH_4$ immersed in an ice-bath while the mixture was stirred vigorously. After the addition of $AgNO_3$ was complete, the resulting pale-yellow solution was stirred continuously at 4 °C for approximately 1 h. The excitation spectra of three batches of the Ag solution prepared in this manner showed an absorbance maximum at 396 nm.

Aqueous sample solutions were prepared by dissolving the tripeptides in deionized water. The concentration of the samples, before mixing with the colloid, was adjusted to 10^{-4} M. The freshly prepared sample solution was added to the silver solution such that the final sample concentration in the silver colloid was $\sim 10^{-5}$ M. The final pH was 8.3.

The SERS spectra of the phosphonate tripeptides were collected twice using each batch of the three silver colloids with a triple-grating spectrometer (Jobin Yvon, T 64000) equipped with a liquid nitrogen-cooled CCD detector (Jobin Yvon, model CCD3000). The spectral resolution was set at 4 cm^{-1}. The 514.5 nm line of an Ar-ion laser (Spectra-Physics, model 2025) was used as an excitation source. Laser power at the sample was set at 20 mW ($\sim$0.5 W/cm^2).

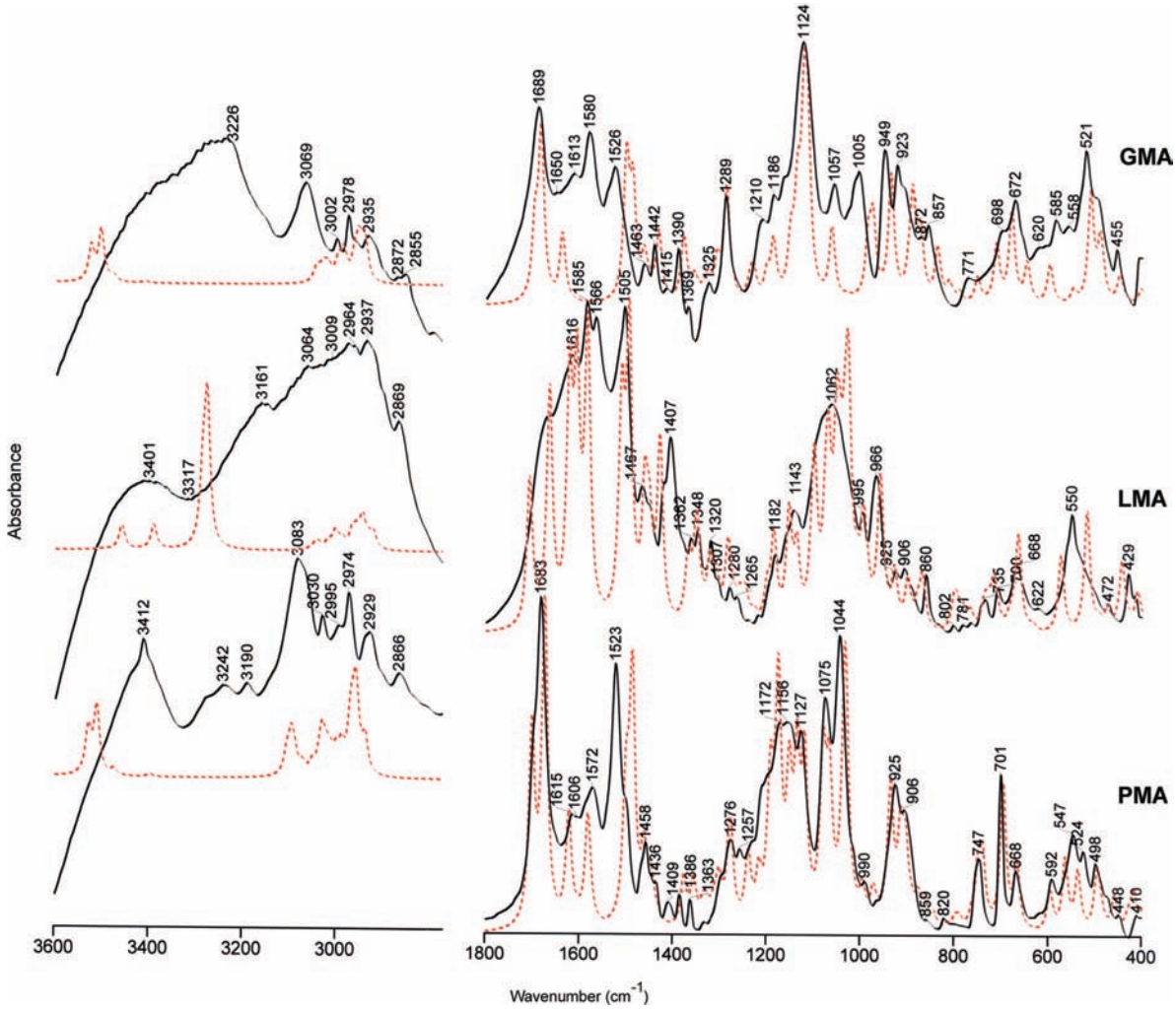

Figure 2. Experimental (solid line) and theoretical (dashed line) FT-IR spectra of L-Gly-L-Met-L-Ala-PO_3H_2 (**GMA**), L-Leu-L-Met-L-Ala-PO_3H_2 (**LMA**), and L-Phe-L-Met-L-Ala-PO_3H_2 (**PMA**) in the spectral range of 3600−400 cm^{-1}.

All of the SERS spectra were recorded within 1 h of the sample's addition to the Ag sol. The spectra obtained were almost identical except for small differences (up to ∼5%) in some band intensities. No spectral changes that could be associated with sample decomposition or desorption processes were observed during these measurements.

Results and Discussion

FT-IR, FT-RS, and DFT Studies. Previously, we have recorded and assigned the Raman spectra of L-Gly-L-Met, L-Leu-L-Met, and L-Phe-L-Met dipeptides and compared them with those of L-Met-L-Gly, L-Met-L-Leu, and L-Met-L-Phe.[36] More recently, we have also provided vibrational characterization of alanine phosphonate dipepides.[23] In the present study, we provide a detailed assignment of the vibrational modes of phosphonate tripeptides consisting of L-Gly-L-Met, L-Leu-L-Met, and L-Phe-L-Met at the N-terminus and P-terminal L-Ala-PO_3H_2, denoted as **GMA**, **LMA**, and **PMA**, based on the results of DFT calculations. These molecules belong to the C_1 point group. Their schematic structures are given in Figure 1. In Figures 2 and 3 are shown the experimental (solid line) and theoretical (dashed-line) FT-IR and FR-RS spectra, respectively, of zwitterionic **GMA**, **LMA**, and **PMA** in the spectral range between 400/200 and 3600 cm^{-1}. The numerical values of the band positions in wavenumbers, together with the proposed band allocations to the normal coordinates, are listed in Table 1. As can be seen from Figures 2 and 3 and from Table 1, the predictions of the DFT methods for the vibrational wavenumbers are in consistently good agreement with the experimental values and allow for the complete assignment of the vibrational modes, which are also in agreement with the previously reported data for constituent amino acids and their di- and tripeptides.[23,36−41]

The assignments of the vibrational bands are somewhat complicated, because these molecules can form many rotamers related to the conformations around the C−C and C−S bonds. However, Som and Mukherjee[42] have shown that it is necessary to consider the conformation around the C−C bond only for the assignment of the vibrational spectra of the molecule in the solid and liquid states. Then, depending on the *trans* (T; the torsion angle $\chi_1 = \pm 180°$) or *gauche* (G; for χ_1 from 0° to 90°) conformation around each bond, several overall rotamers are possible. We used notation proposed by Shimanouchi et al.[43] and Miyazawa et al.[44,45] that includes P_C-T, P_C-G, P_H-T, and P_H-G rotamers, where P_C and P_H refer to the two possible conformations of the $-CH_2CH_2S$ group with the carbon and hydrogen atoms at the trans position with respect to the sulfur atom, respectively, while T and G stand for *trans* and *gauche* internal rotation about the S–CH_2 bond. A medium-strong band at 669 cm^{-1} and a higher-wavenumber shoulder on this spectral feature at 701 cm^{-1} in the FT-RS spectrum of **GMA** (Figure 3, top trace) can be readily assigned to C−S stretching modes of the P_H-T and P_C-G rotamers, respectively. In the FT-IR spectrum

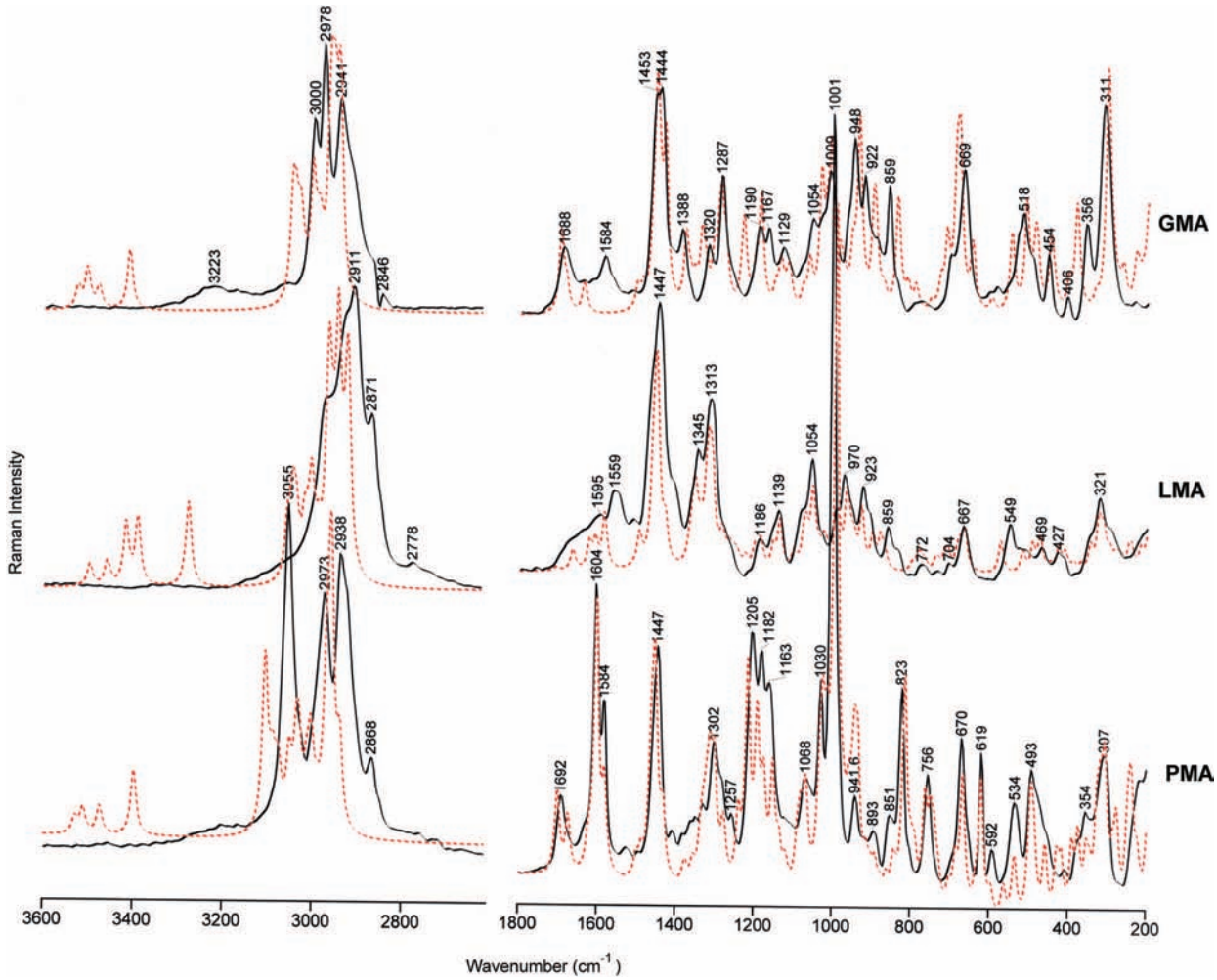

Figure 3. Experimental (solid line) and theoretical (dashed line) (3600−2600 cm^{-1} × 0.3) FT-RS spectra of solid L-Gly-L-Met-L-Ala-PO_3H_2 (**GMA**), L-Leu-L-Met-L-Ala-PO_3H_2 (**LMA**), and L-Phe-L-Met-L-Ala-PO_3H_2 (**PMA**) in the spectral range of 3600−200 cm^{-1}.

of this compound (Figure 2, top trace), two spectral features at 698 and 672 cm^{-1} due to the same conformers of the $-SCH_3$ group can also be observed. At similar wavenumbers, these bands are observed in both the FT-RS and FT-IR spectra of **LMA**, although they show much weaker relative intensities for **LMA** than **GMA** (Figures 2 and 3, middle traces). In the FT-RS spectrum of **PMA** (Figure 3, bottom trace), two medium-intensity bands are clearly observed in the C−S stretching region, namely, the 756 (P_H-G) and 670 cm^{-1} (P_H-T) bands. These bands can be correlated with those at 679 and 729 cm^{-1}, respectively, appearing in the Raman spectrum of L-Phe-L-Met.[36] Such a correlation is partly due to the similarity of the wavenumber and intensity patterns in the same spectral regions of the Raman spectra of the two molecules. However, one must be very cautious, since the CH_2 rocking vibration of the $-CH_2CH_2S$ group may also appear around 750 cm^{-1}. In contrast, three bands at 747, 701, and 668 cm^{-1} of ν(C−S) are easily detected in the **PMA** FT-IR spectrum (Figure 2, bottom trace).

As is generally accepted, most of the FT-IR and FT-RS bands of the studied phosphonate tripeptides can be assigned on the basis of the spectra of their component amino acids.[46−48] However, additional spectral features due to the amide bond vibrations appear. For example, the FT-RS spectra of **GMA**, **LMA**, and **PMA** show a feature due to the amide III mode around 1320−1302 cm^{-1}, a feature that overlaps with other bands present in this region (see Table 1). Rather narrow weak bands at 1688 and 1692 cm^{-1} in the **GMA** and **PMA** FT-RS spectra are assigned to the amide I vibration. In the FT-IR spectra of these molecules, a very strong absorption, at a similar wavenumber, is observed (Figure 2). In the case of **LMA**, the amide I band is hidden under the envelope of bands between 1700 and 1500 cm^{-1} in both the FT-RS and FT-IR spectra. For the amide II there is a strong absorbance at 1526, 1505, and 1523 cm^{-1} for **GMA**, **LMA**, and **PMA**, respectively. The vibration at around 558−534 cm^{-1} could possibly be a mode also associated with some ordered backbone structure of these molecules (amide VI). None of the tripeptides have a clear band in the amide V region around 770 cm^{-1} in the solid state.

Neighboring Raman features at 922 and 859 cm^{-1} (medium enhanced) observed in the **GMA** spectrum (Figure 3, top trace) are assigned to modes dominated by the C−C_A and P−O stretching vibrations, respectively. The 1190 cm^{-1} band of this spectrum is assigned to the P═O stretching mode. In the lower wavenumber range the C−PO_3 deformation mode is identified at 595 cm^{-1}. Moreover, at least four additional bands due mainly to the deformations of the C−PO_3 group (see Table 1 for bands assignment) are expected to appear in the wavenumber range of 500−200 cm^{-1}. Indeed, there are four bands in this range, i.e., 454, 406, 356, and 311 cm^{-1}, with the strongest one appearing at 311 cm^{-1}. The same set of bands is observed in the **GMA** FT-IR spectrum (Figure 2, top trace) as well as in both the FT-IR and FT-RS spectra of **LMA** and **PMA** (Figures 2 and 3).

TABLE 1: Wavenumbes and Band Assignments for FT-RS, FT-IR, and SERS Spectra of Phosphonate Tripeptides Containing P-Terminal L-Met-L-Ala Fragment[a]

calculated wavenumbers (cm^{-1})			assignment B3LYP/6-311++G** (PED > 5%, I > 100 arbitrary units)	experimental wavenumbers (cm^{-1})								
				GMA			LMA			PMA		
GMA	LMA	PMA		FT-RS	FT-IR	SERS	FT-RS	FT-IR	SERS	FT-RS	FT-IR	SERS
262	246		γ(CP(=O,O)OH) (>37), $\rho_b(PO_3)$									
275			$\delta(C(H,N_A)P/C_A)$ (26), $\rho_b(NCH_2C_A)$, $\delta(CC_AO_AN_A)$, $\delta(C_AN_AHC)$				289					
288	296		$\delta(C(H,N_A)P/C_A)$ (>17), $\rho_b(CCH_2C)$ (14), ρ_b(CSC), δ(C−PO_3)									
302	313	302	ν(C−P) (>14), δ(C−PO_3) (>13), ρ_b(CSC), $\rho_b(CCH_2C)$, $\rho_b(CC_AO_AN_A)$, $\delta(C_AN_AHC)$	311			321			307		
		307	γ(C-ϕ) (31), $\rho_b(CC(H)C)_\phi$ (30), $\gamma(\phi)$, ν(C−P), δ(C−PO_3)									
		316	γ(C-ϕ) (34), $\rho_b(CC(H)C)_\phi$ (31), $\gamma(\phi)$, δ(C−PO_3), ρ_b(CSC)									
333	323		$\rho_b(NCH_2C_A)$ (>15), $\delta(CC_AO_AN_A)$, $\delta(C(H,N_A)P/C_A)$, $\delta(C_AN_AHC)$, $\rho_b(CCH_2C)$, $\delta(CC_AO_AN_A)$									
		353	γ(C-ϕ) (40), $\rho_b(CC(H)C)_\phi$, $\gamma(\phi)$, $\rho_b(PO_3)$, γ(CP(=O,O)OH)									
		373	γ(C-ϕ) (35), $\rho_b(CC(H)C)_\phi$ (33), $\gamma(\phi)$, $\delta(PO_3)$, γ(CP(=O,O)OH)	356		340	342			354		334
379	368		$\delta(PO_3)$ (>28), γ(CP(=O,O)OH), $\delta(C(H,N_A)P/C_A)$, $\rho_b(PO_3)$, $\delta(CC_AO_AN_A)$									
382	388		$\rho_b(PO_3)$ (>48), $\delta(PO_3)$, γ(CP(=O,O)OH)									
		389	γ(C-ϕ) (>30), $\rho_b(CC(H)C)_\phi$ (>28), δ(C−PO_3), $\rho_b(CCH_2S)$, $\gamma(\phi)$									
403	409		$\delta(C(H,N_A)P/C_A)$ (>21), δ(C−PO_3), $\rho_b(CCH_2S)$, $\rho_{oop}(CC_AO_AN_A)$, $\rho_{oop}(C_AN_AHC)$	406	408		427	429			410	
		404	$\gamma(\phi)$ (68), $\rho_b(CC(H)C)_\phi$, δ(C−PO_3), $\rho_b(CCH_2S)$, $\rho_{oop}(CC_AO_AN_A)$,									
		416	γ(C-ϕ) (40), $\gamma(\phi)$, $\rho_b(CC(H)C)_\phi$, δ(C−PO_3), $\rho_{oop}(C_AN_AHC)$									
		428	$\gamma(\phi)$ (31), $\rho_b(CC(H)C)_\phi$ (30), γ(C-ϕ)									
440	426		$\delta(PO_3)$ (>18), δ(C−PO_3), $\delta(C(H,N_A)P/C_A)$, $\rho_b(PO_3)$									
448	442		$\delta(C(H,N_A)P/C_A)$ (>29), δ(C−PO_3) (>24), $\rho_{oop}(C_AN_AHC)$	454	455		469	472		452	448	
		458	$\gamma(\phi)$ (38), $\rho_b(CC(H)C)_\phi$ (36), $\delta(PO_3)$, δ(C−PO_3), γ(C-ϕ)									
487	474	487	δ(C−PO_3) (>14), $\rho_{oop}(CC_AO_AN_A)$ (>14), $\rho_{oop}(C_AN_AHC)$, $\gamma(CC_AO_AN_AHC)$, $\delta(C(H,N_A)P/C_A)$,	495	496					493	498	
490	492		$\rho_{oop}(C_AN_AHC)$ (>21), $\rho_{oop}(CC_AO_AN_A)$, $\gamma(CC_AO_AN_AHC)$, $\delta(C(H,N_A)P/C_A)$, δ(C−PO_3)	518	521							
510	517		$\rho_{oop}(C_AN_AHC)$ (>38), $\gamma(CC_AO_AN_AHC)$ (>37)								524	

TABLE 1: Continued

calculated wavenumbers (cm^{-1})			assignment B3LYP/ 6-311++G** (PED > 5%, I > 100 arbitrary units)	experimental wavenumbers (cm^{-1})								
				GMA			LMA			PMA		
GMA	LMA	PMA		FT-RS	FT-IR	SERS	FT-RS	FT-IR	SERS	FT-RS	FT-IR	SERS
		535	$\rho_{oop}(C_AN_AHC)$ (26), $\gamma(\phi)$, $\gamma(CC_AO_AN_AHC)$		558	558	549	550	560	534	547	556
548			$\rho_b(CC_AO_AN_A)$ (20), $\delta(C(H,N_A)P/C_A)$									
598	573	620	$\rho_{oop}(CC_AO_AN_A)$ (>20) $\gamma(CC_AO_AN_AHC)$, $\nu(C-C_A)$, $\delta(CC_AO_AN_A)$, $\delta(NCH_2C_A)$, $\delta(CCH_2C)$		585					592	592	
		634	$\gamma(\phi)$ (21), $\delta(\phi)$, $\sigma_{oop}(CC(C)C)_\phi$, $\nu(C-P)$							619		612
647	664		$\delta(CC_AO_AN_A)$ (>26), $\delta(C(H,N_A)P/C_A)$, $\nu(C-P)$, $\rho_{oop}(CC_AO_AN_A)$		620	608		622				
680	676	666	$\nu(C-P)$ (>22), $\nu(C-S)$, $\nu(P-O)$	669	672	671	667	668	673	670	668	672
688	684	685	$\nu(C-S)$ (>73)									
	706		$\nu(C-S)$ (29), $\rho_b(NCH_2C_A)$, $\delta(CCH_2C)$									
712	711	729	$\nu(C-S)$ (>37), $\delta(CCH_2C)$, $\rho_b(NCH_2C_A)$, $\delta(C(H,N_A)P/C_A)$	701	698		704	708			701	
729	737		$\nu(C-S)$ (>56), $\rho_{oop}(CC_AO_AN_A)$, $\nu(C-C)$							756	747	
752	765	814	$\rho_{oop}(CC_AO_AN_A)$ (>30), $\nu(C-S)$, $\delta(CCH_2C)$		771		772					
791	775		$\delta(CCH_2S)$ (>33), $\delta(CCH_2C)$,$\rho_{oop}(CC_AO_AN_A)$, $\delta(C(H,N_A)P/C_A)$			799			792			788
812	801		$\nu(P-O)$ (>60), $\nu(C-P)$, $\rho_b(POH)$			831				823	820	829
837			$\nu(P-O)$ (82), $\rho_b(POH)$	859	857	860	859	860	877	851		857
		861	$\rho_b(CC(H)C)_\phi$ (53), $\gamma(\phi)$ (41)									
873	879		$\rho_{oop}(C-NH_3^+)$ (>48), $\nu(N-C)$, $\delta(CC_AO_AN_A)$									
		876	$\rho_b(CC(H)C)_\phi$ (48), $\gamma(\phi)$ (44), $\gamma(C\text{-}\phi)$, $\rho_{oop}(C-NH_3^+)$, $\nu(N-C)$									
890			$\delta(NCH_2C_A)$ (37), $\rho_b(C-NH_3^+)$, $\rho_{oop}(CC_AO_AN_A)$, $\rho_{oop}(C-NH_3^+)$	892	907		906	906		893	906	
893			$\delta(C-CH_3)$ (20), $\nu(C-C)$ (18), $\nu(C-N_A)$, $\rho_b(C-CH_3)$, $\delta(C_AN_AHC)$									
890	899		$\delta(NCH_2C_A)$ (>16), $\nu(C-C_A)$, $\nu(C-C)$, $\rho_b(C-NH_3^+)$, $\rho_{oop}(CC_AO_AN_A)$, $\delta(CCH_2S)$									
		889	$\gamma(\phi)$ (49), $\rho_b(CC(H)C)_\phi$, $\delta_{oop}(CNH_3^+)$, $\nu(C-C)$, $\rho_b(CCH_3)$									
		902	$\gamma(\phi)$ (50), $\rho_b(CC(H)C)_\phi$, $\gamma(C\text{-}\phi)$, $\nu(C-CH_3)$, $\delta(C-CH_3)$, $\delta(CC_AO_AN_A)$, $\rho_b(C-CH_3)$									
		933	$\rho_b(POH)$ (49), $\rho_b(CC(H)C)_\phi$, $\gamma(\phi)$									
935	927		$\nu(C-C_A)$ (>25), $\rho_{oop}(C-NH_3^+)$, $\delta(CC_AO_AN_A)$, $\delta(CCH_2S)$, $\delta(S-CH_3)$, $\delta(CCH_2C)$, $\delta(C_AN_AHC)$	922	923	915	923	925	910		925	
951	947		$\delta(S-CH_3)$ (>70), $\nu(C-C)$, $\rho_b(S-CH_3)$									
954	965		$\rho_b(S-CH_3)$ (>63), $\delta(S-CH_3)$, $\nu(C-C)$	948	949	949	970	966	949	941		949
		971	$\rho_b(POH)$ (46), $\gamma(\phi)$								990	
974	985		$\rho_b(POH)$ (>86)									
985	993		$\rho_b(POH)$ (>78)									
1007	1007		$\nu(C-C)$ (>35), $\nu(C-C_A)$, $\delta(CCH_2C)$, $\delta(CCH_2S)$	1009	1005		990	995				
		1014	$\gamma(C\text{-}\phi)$ (47), $\rho_b(CC(H)C)_\phi$							1001		1003
	1018		$\nu(C-C)$ (25), $\delta(CCH_2S)$, $\delta(CCH_2C)$, $\delta(C-CH_3)$									

TABLE 1: Continued

calculated wavenumbers (cm^{-1})			assignment B3LYP/6-311++G** (PED > 5%, I > 100 arbitrary units)	experimental wavenumbers (cm^{-1})								
				GMA			LMA			PMA		
GMA	LMA	PMA		FT-RS	FT-IR	SERS	FT-RS	FT-IR	SERS	FT-RS	FT-IR	SERS
1018	1022		ν(C−C) (>16), $\delta(CCH_2S)$, $\delta(CCH_2C)$, $\delta(C-CH_3)$, $\rho_b(C-CH_3)$, $\nu(C-N_A)$									
1030	1026		ν(C−C) (>38), $\rho_b(C-CH_3)$, $\rho_b(S-CH_3)$							1030		
1033	1035		ν(C−C) (>27), $\rho_b(C-CH_3)$, $\delta(C-CH_3)$, $\nu(C-N_A)$								1044	1052
1062	1068		$\nu(C-N_A)$ (>28), ν(C−C), ν(N−C), $\delta(C-CH_3)$	1054	1057	1048	1054	1062		1068	1075	
		1063	γ(C-ϕ) (52), $\rho_b(CC(H)C)_\phi$, $\nu(C-C)_{CH_3}$, $\nu(N_A-C)$, ν(N−C), $\rho_b(C-CH_3)$									
1079	1074		ν(C−C) (>22), $\nu(C-N_A)$ (>22), ν(N−C), $\delta(C-CH_3)$									
1113	1097		ν(N−C) (>49), $\nu(C-N_A)$, $\delta(NCH_2C_A)$, $\rho_b(NCH_2C_A)$, $\rho_{oop}(C-NH_3^+)$									
	1101	1118	$\rho_b(CC(H)C_A)$ (>15), $\rho_b(C-CH_3)$, $\nu(C-N_A)$, $\delta(CCH_2S)$, $\delta(CCH_2C)$	1129	1124		1139	1143	1051		1127	1133
1122			$\delta(CCH_2S)$ (16), $\delta(CCH_2C)$, $\rho_b(C-CH_3)$, $\delta(CC(H,N_A)P/C_A)$, $\nu(C-N_A)$, $\rho_b(C(H,N_A)P/C_A)$									
		1135	$\rho_b(CC(-H)C)_\phi$ (20), γ(C-ϕ), $\delta(CCH_2S)$, $\nu(C-N_A)$, $\delta(CCH_2C)$									
1136	1135		$\nu(C-N_A)$ (>15), $\delta(CCH_2S)$ (>15), $\delta(CCH_2C)$, $\rho_b(C-CH_3)$, $\delta(NCH_2C_A)$									
		1151	$\nu(C-C)_\phi$ (32), γ(C-ϕ) (24), $\rho_b(CC(-H)C)_\phi$ (23)									
1150	1152		$\delta(NCH_2C_A)$ (>32), $\rho_b(C-NH_3^+)$, $\nu(C-N_A)$									
		1175	γ(C-ϕ) (39), $\rho_b(CC(H)C)_\phi$ (37)									
1187	1184		$\nu(C-N)_A$ (>36), $\rho_b(C_AN_AHC)$, $\rho_b(C(H,N_A)P/C_A)$	1167	1164				1175	1163	1156	1168
		1190	γ(C-ϕ) (34), $\rho_b(CC(-H)C)_\phi$ (31), $\nu(C-N)_A$									
1201	1199		$\nu(C-N)_A$ (>27), $\rho_b(C_AN_AHC)$, $\delta(CC_AO_AN_A)$									
1230	1222		ν(P═O) (>73), $\rho_b(C(H,N_A)P/C_A)$	1190	1186	1190	1186	1182	1192	1182	1172	1190
		1238	ν(P═O) (44) $\rho_b(C(H,N_A)P/C_A)$, $\delta(CC(H,N_A)P/C_A)$									
		1215	γ(C-ϕ) (46), $\rho_b(CC(-H)C)_\phi$ (40)							1205	1209	
1238	1247		$\delta(CCH_2S)$ (>57), $\delta(CCH_2C)$, $\rho_b(C(H,N_A)P/C_A)$		1210							
		1239	$\delta(CCH_2S)$ (50), $\delta(CCH_2C)$									
	1267	1275	ν(P═O) (>26), $\rho_b(C(H,N_A)P/C_A)$, $\nu(C-C)_\phi$, $\delta(CCH_2S)$					1264		1257	1251	
1276	1280		$\delta(CCH_2S)$ (>27), $\delta(CCH_2C)$ (>27), $\delta(CC(H,N_A)P/C_A)$									
1287	1285		$\rho_b(C(H,N_A)P/C_A)$ (>48), ν(P═O), $\delta(CC(H,N_A)P/C_A)$, ν(C−P)									
1294			$\delta(CC(H,N_A)P/C_A)$ (43), $\rho_b(C(H,N_A)P/C_A)$, $\delta(CCH_2C)$	1287	1289	1270		1280	1278		1276	1270
−	−	1298	γ(C-ϕ) (34), $\rho_b(CC(-H)C)_\phi$ (32)									
		1301	γ(C-ϕ) (28), $\rho_b(CC(-H)C)_\phi$ (21), $\delta(CCH_2C)$, $\delta(CCH_2S)$, $\delta(CC(H,N_A)P/C_A)$									
1307	1308		$\delta(CC(H,N_A)P/C_A)$ (>37), $\rho_b(C_{=O}N_A(H)C_s)$, $\delta(CCH_2S)$, $\rho_b(C(H,N_A)P/C_A)$, $\delta(S-CH_3)$, $\delta(NCH_2C_A)$									

TABLE 1: Continued

calculated wavenumbers (cm^{-1})			assignment B3LYP/6-311++G** (PED > 5%, *I* > 100 arbitrary units)	experimental wavenumbers (cm^{-1})								
				GMA			LMA			PMA		
GMA	LMA	PMA		FT-RS	FT-IR	SERS	FT-RS	FT-IR	SERS	FT-RS	FT-IR	SERS
	1314		$\nu(C-N)_A$ (22), $\rho_b(C_{=O}N_A(H)C_s)$									
	1318	1310	$\delta(CC(H,N_A)P/C_A)$ (>40), $\delta(CCH_2C)$									
		1316	$\gamma(C\text{-}\phi)$ (49), $\rho_b(CC(-H)C)_\phi$ (34), $\delta(CCH_2C)$					1305		1302	1294	
	1322	1321	$\delta(NC(H,C)C_A)$ (>23), $\nu(C-N)_A$, $\delta(S-CH_3)$, $\delta(CCH_2C)$, $\rho_b(C-NH_3^+)$									
1325	1325		$\rho_b(C_AN_A(H)C_s)$ (>20), $\nu(C-N)_A$, $\delta(N_AC_s(H,P)C)$	1320	1325	1318	1313	1320				1315
		1327	$\rho_b(CC(H)C_A)$ (27), $\delta(S-CH_3)$, $\delta(CC(H,N_A)P/C_A)$, $\delta(CCH_2C)$, $\gamma(C_AN_AHC(H,C)P/C_A)$									
1330			$\delta(CC(H,N_A)P/C_A)$ (28), $\delta(NCH_2C_A)$, $\delta(S-CH_3)$, $\delta(CCH_2C)$									
		1333	$\gamma(C\text{-}\phi)$ (39), $\rho_b(CC(-H)C)_\phi$ (37)									
		1336	$\gamma(C\text{-}\phi)$ (29), $\rho_b(CC(-H)C)_\phi$ (23), $\delta(S-CH_3)$, $\delta(NC(H,C)C_A)$									
1338	1338		$\delta(CCH_2C)$ (>25), $\delta(CC(H,N_A)P/C_A)$, $\delta(S-CH_3)$, $\delta(NCH_2C_A)$, $\delta(CCH_2S)$									
	1349		$\delta(CCH_2C)$ (22), $\rho_b(C-NH_3^+)$, $\delta(NCH_2C_A)$, $\rho_b(C(H,N_A)P/C_A)$		1369		1345	1348				
		1355	$\delta(CCH_2C)$ (16), $\rho_b(NC(H)C_A)$, $\delta(NC(H,C)C_A)$					1362			1363	
1367	1359		$\delta(NCH_2C_A)$ (>31), $\rho_b(C-NH_3^+)$, $\rho_b(C(H,N_A)P/C_A)$, $\delta(CCH_2C)$, $\nu(C-C_A)$									
1378	1368		$\delta(C-CH_3)$ (>53), $\nu(C-C)$, $\nu(C=O)$	1388	1390	1387		1407	1391		1386	1389
1410	1398		$\delta(C-CH_3)$ (>43), $\rho_b(NC(H)C_A)$		1415		1410	1420	1409			
		1376	$\delta(C-CH_3)$ (35), $\rho_b(NC(H)C_A)$, $\gamma(C\text{-}\phi)$								1409	
1432	1428	1431	$\delta(CH_3)$ (>62), $\rho_b(CH_3)$	1444	1442	1443	1447	1455	1447	1447	1436	
1432		1444	$\rho_b(NCH_2C_A)$ (91)									
		1444	$\gamma(C\text{-}\phi)$(27), $\nu(C-C)_\phi$, $\rho_b(CCH_2C)$, $\gamma(\phi)$									
1447	1447	1448	$\rho_b(CH_3)$ (>51), $\delta(CH_3)$									
		1453	$\rho_b(CCH_2C)$ (38), $\gamma(C\text{-}\phi)$									
1453	1451	1453	$\rho_b(CCH_2C)$ (>70), $\rho_b(CCH_2S)$	1453	1463	1463	1459	1467			1458	1458
		1460	$\rho_b(CH_3)$ (62) $\delta(CH_3)$, $\delta(C-CH_3)$									
1456	1453		$\rho_b(CH_3)$ (>84), $\delta(C-CH_3)$									
1462	1459	1461	$\delta(CH_3)$ (>41), $\rho_b(CH_3)$, $\rho_b(CCH_2S)$, $\rho_b(C-CH_3)$									
	1460	1463	$\rho_b(CCH_2S)$ (>55), $\delta(CH_3)$, $\rho_b(CCH_2C)$									
1463	1461		$\delta(CH_3)$ (>60), $\rho_b(CCH_2S)$, $\rho_b(CCH_2C)$, $\rho_b(C-CH_3)$									
		1488	$\nu(C-C)_\phi$ (35), $\rho_b(C_AN_AHC)$, $\nu(C-N)_A$, $\gamma(C\text{-}\phi)$								1502	
1488	1495	1486	$\rho_b(C_AN_AHC)$ (>35), $\nu(C-N)_A$, $\nu(C-N_A)$		15261580			1505	1519		1523	
1502		1500	$\rho_b(C_AN_AHC)$ (>31), $\nu(C-N)_A$, $\nu(C-N_A)$, $\delta(CC(H,N_A)P/C_A)$		1580			1566				
		1581	$\nu(C-C)_\phi$ (80), $\rho_{ipb}(CC(-H)C)_\phi$, $\delta\phi$							1584	1572	1587
		1602	$\nu(C-C)_\phi$ (82), $\rho_{ipb}(CC(-H)C)_\phi$, $\delta\phi$							1604	1615	1604
1638	1622	1622	$\delta(C-NH_3^+)$ (>91)	1584	1613		1595	1585				
1683	1664	1673	$\nu(C=O)_A$ (>66)			1586		1616	1584			
1697	1707	1700	ν $(C=O)_A$ (>75), $\nu(C_A-N_A)$, $\rho_b(CN_A(H)C_A)$	1688	1689	1622		1668	1634	1692	1683	1696

TABLE 1: Continued

calculated wavenumbers (cm^{-1})			assignment B3LYP/ 6-311++G** (PED > 5%, I > 100 arbitrary units)	experimental wavenumbers (cm^{-1})								
				GMA			LMA			PMA		
GMA	LMA	PMA		FT-RS	FT-IR	SERS	FT-RS	FT-IR	SERS	FT-RS	FT-IR	SERS
	2925		$\nu(C-H)_{CH_2}$ (91)									
	2934		$\nu(C-H)_{CH_2}$ (93)									
2945	2945	2938	$\nu(C-H)_{CH_2}$ (>95)		2855							
2956	2957	2958	$\nu(C-H)_{CH_3}$ (>89)		2872	2867	2871	2869	2873	2868	2866	2873
2964	2966	2961	$\nu(C-H)_{CH_3}$ (>99)				2911					
2986	2988	2988	$\nu(C-H)$ (>82), $\nu(C-H)_{CH_2}$	2941	2935	2929	2927	2937	2930	2938	2929	2938
2992	2990		$\nu(C-H)$ (>76), $\nu(C-H)_{CH_2}$	2978	2978	2976	2970	2964		2973	2974	
3002	3003	2999	$\nu(C-H)$ (>91)								2995	2989
3021	3019	3020	$\nu(C-H)_{CH_2}$ (>89)	3000	3002			3009				
3030	3020	3029	$\nu(C-H)_{CH_3}$ (>96)									
3033	3038	3036	$\nu(C-H)_{CH_3}$(100)									
3042	3045	3045	$\nu(C-H)_{CH_2}$ (>54)									
3049	3049	3051	$\nu(C-H)$ (>92)	3047	3069			3064				
	3058	3077	$\nu(C-H)_{CH_3}$ (>96)					3161	3161			
		3088	$\nu(C-H)_{\phi}$ (95)							3055	3030	
		3096	$\nu(C-H)_{\phi}$ (96)								3083	
		3105	$\nu(C-H)_{\phi}$ (95)								3190	
3412	3418	3398	$\nu(N-H)$ (100)	3223	3226	3227		3401	3230		3242	3231
3480	3460	3474	$\nu(N-H)$ (99)			3473			3478	3455	3412	3475
3506	3499	3511	$\nu(N-H)_A$ (99)									
3527		3529	$\nu(N-H)_A$ (99)									
3727		3718	$\nu(O-H)$ (100)									
3728	3738	3735	$\nu(O-H)$ (100)									

[a] Legend: ν, stretching; δ, deformation; ρ_b, bending deformation; ρ_{oop}, out-of-plane bending; ρ_{inp}, in-plane bending, γ, torsion; C_A, the carbon atom of the amide bond; N_A, the nitrogen atom of the amide bond; O_A, the oxygen atom of the amide bond; ϕ, the Phe aromatic ring; and $(...)_{CH_3}$ and $(...)_{CH_2}$, the fragment of the methyl and methylene group, respectively.

The spectra of all investigated tripeptides also show several common bands at 970−948, 1075−1048, 1154−1123, ∼1165, and ∼1287 cm^{-1} (see Table 1 for detailed band positions). The former band is most probably due to the S−CH_3 vibrational coordinates. The 1075−1048 and 1154−1123 cm^{-1} features involve the –CH_3 group mode coupled with ν(C−C) and $\nu(C-N_A) + \delta(CCH_2S/C)$. The C−N stretching mode mixes with other modes, $\delta(NCH_2C_A) + \rho_b(C-NH_2)$, giving rise to a band at ∼1165 cm^{-1}. This latter band is due to the $\delta(CCH_2S/C) + \delta(CC(H,N_A)P/C_A)$ modes.

Other important bands that are observed and presented in the spectra shown in Figures 2 and 3 can be assigned as follows. A very complex spectral pattern of the molecules precludes clear assignment of most of the NH_3^+ vibrations, due to their low intensity in the FT-RS spectra. However, two bands at 1616−1584 and 1369−1345 cm^{-1} are probably due to the C−NH_3^+ deformation and the CCH_2C deformation coupled with the C−NH_3^+ bending, respectively. It seems reasonable to assign two of the most pronounced bands observed, at 1453 and 1444 cm^{-1}, to the CH_3 and CH_3/CH_2 deformations. In addition, two bands are frequently observed near 1415 and 1390 cm^{-1}. The former band is assigned mainly to the $\delta(C-CH_3) + \rho_b(NC(H)-C_A)$ mode, while we assume that the latter band overlaps with one or two bands that arise from the $\delta(C-CH_3)$, ν(C−C), and ν(C═O) modes. Other skeletal C−C stretching modes are grouped in the 1100−900 cm^{-1} region.

The bottom trace in Figure 3 depicts the FT-RS spectrum of **PMA** tripeptide containing N-terminal L-Phe. The characteristic L-Phe aromatic ring bands appear in the spectrum of Phe at 619, 1001, 1030, 1182, 1205, 1584, and 1604 cm^{-1} and are assigned to the in-plane ring deformation (ν_{6b}), symmetric ring breathing (ν_{12}), in-plane CH bending (ν_{18a}), combination of in-plane CH bending (ν_{9a}) with ring stretching, phenyl-C stretching (ν_{7a}), and two in-plane ring stretching vibrations (ν_{8b} and ν_{8a}), respectively.[46,49−51] It is notable that the above-mentioned features closely resemble previously reported spectra of L-Phe and its homo- and heterodimers.[36,37]

SERS Study. Figure 4 shows the SERS spectra of **GMA**, **LMA**, and **PMA** adsorbed on the colloidal silver at pH ∼8.3. At this pH, the investigated tripeptides form anionic species, i.e., N- and P-terminal groups are deprotonated (−NH_2 and −PO_3H^-). The observed wavenumbers, together with the proposed SERS band assignments, are summarized in Table 1. The allocation of SERS bands to the normal vibrations for these tripeptides was done on the grounds of previously reported assignments cited for L-Gly-L-Met, L-Leu-L-Met, and L-Phe-L-Met dipeptides[36] and Ala-containing phosphonate dipeptides[23] as well as on the grounds of PED (potential energy distribution) analysis of FT-RS spectra (in terms of normal coordinates) performed in this work.

The SERS spectra of these molecules (Figure 4) are very different from their corresponding FT-RS spectra (Figure 3). For example, the strong Raman bands ascribable to CH_3 and CH_2 deformations, coupled modes of the CCH_2S/C and $CC(H-,N_A)P/C_A$ deformations, and C−C stretching vibrations, which appear at 1453/1444, 1287, and 1009 cm^{-1}, respectively, decrease or even disappear from the SERS spectra. By contrast, in the SERS spectra the strongest 1190 and 671 cm^{-1} bands due to ν(P═O) and ν(C−S), respectively, are enhanced. On the other hand, we note distinctive similarities between the SERS spectra of these three phosphonate tripeptides. This points out that substitution of L-Gly in **GMA** by L-Leu (**LMA**) or L-Phe (**PMA**) does not influence the adsorption mechanism of these tripeptides on the colloidal silver nanoparticles. However, in the case of **PMA**, additional bands due to the L-Phe/Ag complex formation are enhanced. This is not surprising, however, since it has been proven that an aromatic ring of molecules preferentially binds to a metal surface.[10,25,52]

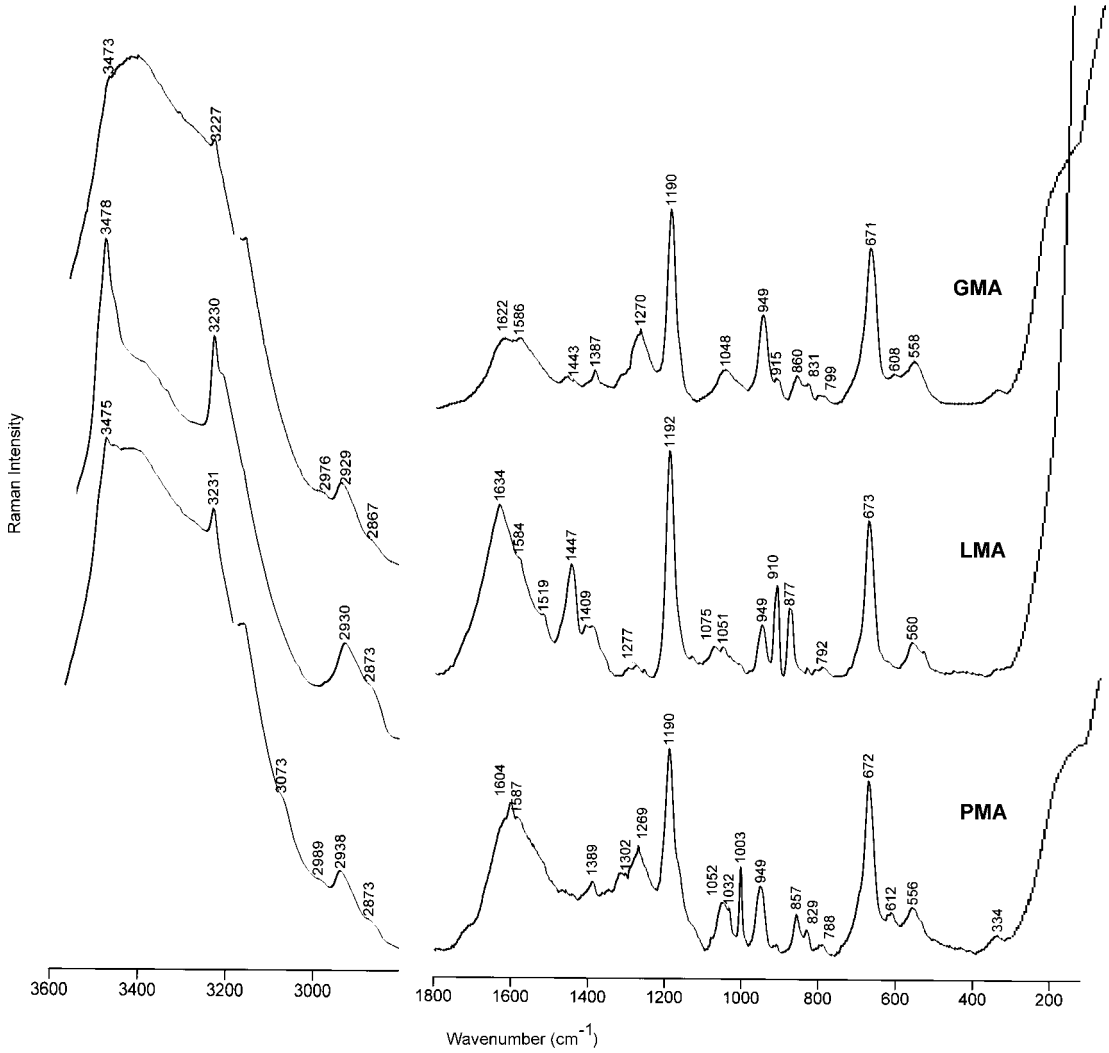

Figure 4. SERS spectra of L-Gly-L-Met-L-Ala-PO_3H_2 (**GMA**), L-Leu-L-Met-L-Ala-PO_3H_2 (**LMA**), and L-Phe-L-Met-L-Ala-PO_3H_2 (**PMA**) adsorbed on a colloidal silver surface in the spectral range of 3600−190 cm^{-1}.

As mentioned above, the SERS spectra of **GMA**, **LMA**, and **PMA** adsorbed on the silver surface show two strongly enhanced bands at 1190 and 673 cm^{-1} of the ν(P═O) and ν(C−S) (P_H-T conformer) modes. These bands exhibit comparable relative intensities and band widths between the SERS spectra [fwhm (full width at half-maximum) = 24−26 cm^{-1} for ν(P═O) and fwhm = 29−33 cm^{-1} for ν(C−S)]. In addition, for **GMA** both these bands do not move (Δ_ν = 0−2 cm^{-1}) (Figure 4, top trace), while for the other two tripeptides they shift slightly up by 6−8 cm^{-1}. These findings indicate that the P═O and C−S bonds strongly interact, adopting a flat orientation with respect to the colloidal silver surface. They also show that the strength of this interaction is comparable between molecules and that the most abundant conformer is not dependent on the composition of the investigated tripeptides. Thus, these SERS spectra clearly indicate the same pattern of interaction between the $-SCH_3$ fragment of L-Met in the investigated compound and the colloidal silver particles. Additional support for the idea that the sulfur atom interacts with the silver surface comes from the presence of the 949 cm^{-1} band assigned to the S−CH_3 deformation. It should be emphasized that the enhancement of this mode is slightly larger for **GMA** than for **PMA** or **LMA**, due to slight alternations for these molecules in the geometry of their S−CH_3 fragments on the surface.

Also, the P−O stretching vibrations at 860, 877, and 857 cm^{-1} are enhanced in the SERS spectra of **GMA**, **LMA**, and **PMA**, respectively. A rather weak relative intensity for this band is observed for **GMA** and **PMA**, while in the case of **LMA** it exhibits medium relative intensity. This medium intensity can only be explained by assuming that the P−O bond assists in the interaction with the silver surface, adopting a tilted orientation with respect to it.

Several studies considered normal mode assignments of specific modes to bands of the SERS spectra from surface-bound phosphate anions on silver colloids[53,54] and electrodes.[55,56] However, these investigations remain controversal; they assigned a low-wavenumber band at around 230−320 cm^{-1}, which is absent in the phosphate anions normal Raman spectra, to the formation of the metal−anion bond.[57,58] Because this band is far below the expected internal vibrational modes of adsorbed phosphate anions, it is assigned to the stretching mode of a phosphate oxygen−Ag bond, ν(Ag−O). This spectral feature usually is observed as an intense and broad band in the SERS spectra of chemisorbed species.[57,58] The SERS spectra of **GMA** and **PMA** shown in Figure 4 reveal at 205 and 195 cm^{-1}, respectively, the band of this mode. For **LMA** the position of this band is lower. The observed wavenumber shifts are in accord with the view that coordination with the Ag surface decreases the double-bond character of the P−O (surface-

coordinated oxygen atom) bond, which causes an increase in bond length and a decrease in corresponding wavenumber. Therefore, it can be stated that the double-bond character of the P−O bond decreases in the following order: **GMA** > **PMA** > **LMA**.

The SERS spectra of **GMA** and **PMA** also yield medium enhanced spectral features due to the amide I, III, and IV vibrations around 1610−1634, ∼1270, and ∼558 cm^{-1}, respectively, which are detected as a single, broad band, except for the vibrations from amide I, the band which overlaps with the ν_{as}(C═O) mode and the L-Phe modes in the case of **PMA**. Among these, the amide I and IV are clearly observed in the SERS spectrum of **LMA**, while the amide III mode is negligibly enhanced in its spectrum. Of particular note is that the relative intensity of the amide I band decreases in the SERS spectra in this direction: **GMA** < **PMA** < **LMA**. Simultaneously, the relative intensity of the amide III band decreases in the opposite direction (**LMA** < **PMA** < **GMA**). Considering the fact that the amide III band arises mainly from a combination of the in-phase and out-of-phase N−H bending and C−N stretching, whereas amide I mainly involves the C═O stretching, C_α−C−N deformation, and C−N stretching oscillations,[59] it can be proposed that the −CONH− fragment of each molecule assists in their interaction with the colloidal silver surface in slightly different fashions. It adopts a tilted orientation with respect to this surface for all tripeptides; however, the C═O unit of the **LMA** peptide bond is closer to the silver nanoparticles than the N−H moiety of this bond. The reverse situation is observed in the case of **GMA**. The C═O···Ag interaction is supported by the SERS medium enhancement of the $\nu_s(C-C_A)$ mode at 910 cm^{-1} and ν(C═O) at 1409 cm^{-1}, and at around 1584 cm^{-1} in the **LMA** SERS spectrum (Figure 4, middle trace). In comparison, a very weak enhancement of 915 and 1387 cm^{-1} SERS signals is observed for **GMA** (Figure 4, top trace), while the ∼1586 cm^{-1} band decreases in its relative intensity compared to **LMA**.

In the SERS spectra of all phosphonate tripeptides deposited onto the colloidal silver surface, the enhancement of bands due to the methyl group is also observed. Thus, it seems obvious that this group gives SERS signals at ∼1443 [$\delta(CH_3)$ + $\rho_b(CH_3)$] and ∼1051 cm^{-1} [$\delta(CH_3)$ + ν(C−C)] (see Table 1 for detailed band positions). The former spectral feature is enhanced for **LMA** compared to **GMA** and **PMA**. The latter one exhibits similar weak relative intensity for all tripeptides. Thus, it may be concluded that **LMA** also interacts with the silver surface through the methyl group, while this group for **GMA** and **PMA** lies in proximity to the surface.

As in the case of L-Phe and L-Phe-L-Met and L-Met-L-Phe dipeptides adsorbed on the silver surface,[36,37] the aromatic ring of **PMA** gives rise to several well-defined SERS bands, i.e., 1604 (ν_{8a}), 1587 (ν_{8b}), 1032 (ν_{18a}), 1003 (ν_{12}), and 621 (ν_{6b}) cm^{-1}. All of these bands exhibit low intensity, suggesting that the phenyl rings of **PMA** are oriented nearly horizontally to the silver surface. Additionally, there is no wavenumbers shift of these bands when compared to their positions in the FT-RS spectrum, implying no direct interaction between L-Phe and Ag.

Conclusions

SERS spectra of the anionic species (pH ∼8.3) of **GMA**, **LMA**, and **PMA** deposited onto a colloidal silver surface are presented in this work. Their adsorption patterns were investigated from the intensities and wavenumbers of the enhanced bands. We showed that these molecules bind through the P═O and C−S bonds with similar strength to the silver surface through lone electron pairs on the sulfur and oxygen atoms. In addition, the pattern of the SERS spectra provides strong evidence that the −CONH− bond of all molecules adopts a tilted orientation on the silver surface. In this geometry, the C═O unit of **LMA** interacts more strongly with the silver surface than the N−H unit, while the reverse is seen for **GMA**. This is probably due to distance effects. Additionally, the P−O bond and CH_3 group of **LMA** assist in the adsorption process of this molecule. On the other hand, the Phe aromatic ring (in tilted close to horizontal orientation with regard to the silver surface) of **PMA** assists in the adsorption process.

Regarding the density functional theory method employed, it can be demonstrated again that quantum chemical calculations are successful in modeling the molecular structures of small peptides. Additionally, the PCM model is found to work very well for the phosphonate tripeptides in their zwitterionic form, resulting in structures capable of reproducing the experimental vibrational spectra.

Acknowledgment. This work was supported by the Polish State Committee for Scientific Research (Grant No. 1 T09A 112 30 to E.P.). The authors are grateful to the Academic Computer Center "Cyfronet" in Krakow for allowing us to conduct all calculations presented in this work.

References and Notes

(1) Allen, J. S.; Atherton, F. R.; Hall, M. J.; Hassall, C. H.; Holmes, S. W.; Lambert, R. W.; Nisbet, L. J.; Ringrose, P. S. *Nature* **1978**, *272*, 56.
(2) Kametani, T.; Suzuki, Y.; Kisagawa, K.; Hiiragi, H.; Wakisaka, K.; Haga, S.; Irino, O.; Saita, O.; Yamabe, S. *Heterocycles* **1982**, *18*, 295.
(3) Atherton, F. R.; Hassall, C. H.; Lambert, R. W. *J. Med. Chem.* **1986**, *29*, 29.
(4) Payne, J. W. *Biochem. Soc. Trans.* **1983**, *11*, 794.
(5) Zboińska, E.; Sztajer, H.; Lejczak, B.; Kafarski, P. *FEMS Microbiol. Lett.* **1993**, *108*, 225.
(6) Haris, P. I.; Severcan, F. *J. Mol. Catal. B: Enzym.* **1999**, *7*, 207.
(7) Dong, A.; Meyer, J. D.; Kendrick, B. S.; Manning, M. C.; Carpenter, J. F. *Arch. Biochem. Biophys.* **1996**, *334*, 406.
(8) Petrelski, S.; Tedeschi, N.; Arakawa, T.; Carpenter, J. F. *Biophys. J.* **1993**, *65*, 661.
(9) Yeh, H. C.; Chao, S. Y.; Ho, Y. P.; Wang, T. H. *Curr. Pharm. Biotechnol.* **2005**, *6*, 453.
(10) Podstawka, E.; Ozaki, Y.; Proniewicz, L. M. *Appl. Spectrosc.* **2005**, *59*, 1516.
(11) Shanmukh, S.; Jones, L.; Driskell, J.; Zhao, Y.; Dluhy, R.; Tripp, R. A. *Nano Lett.* **2006**, *6*, 2630.
(12) Podstawka, E.; Sikorska, E.; Proniewicz, L. M.; Lammek, B. *Biopolymers* **2006**, *83*, 193.
(13) MacBeath, G.; Schreiber, S. L. *Science* **2000**, *289*, 1760.
(14) Yonzon, Ch. R.; HaynesCh. L.; Zhang, X.; Walsh, J. T., Jr.; Van Duyne, R. P. *Anal. Chem.* **2004**, *76*, 78.
(15) Tada, H.; Bronkema, J.; Bell, A. T. *Catal. Lett.* **2004**, *92*, 93.
(16) Li, H.; Sun, J.; Cullum, B. M. *Nanobiotechnology* **2006**, *2*, 17.
(17) Volny, M.; Elam, W. T.; Ratner, B. D.; Turecek, F. *J. Biomed. Mater. Res. B: Appl. Biomater.* **2006**, *80B*, 505.
(18) Pradier, C. M.; Salmain, M.; Zheng, L.; Jaouen, G. *Surf. Sci.* **2002**, *502/503*, 193.
(19) Grubisha, D. S.; Lipert, R. J.; Park, H.-Y.; Driskell, J.; Porter, M. D. *Anal. Chem.* **2003**, *75*, 5936.
(20) Hodneland, C. D.; Lee, Y.-S.; Min, D.-H.; Mrksich, M. *Proc. Natl. Acad. Sci. U.S.A.* **2002**, *99*, 5048.
(21) Kubelka, J.; Keiderling, T. A. *J. Am. Chem. Soc.* **2001**, *123*, 12048.
(22) Podstawka, E.; Kudelski, A.; Proniewicz, L. M. *Surf. Sci.* **2007**, *601*, 4971.
(23) Podstawka, E.; Andrzejak, M.; Kafarski, P.; Proniewicz, L. M. *J. Raman Spectrosc.* **2008**, *39*, 1238.
(24) Podstawka, E.; Kafarski, P.; Proniewicz, L. M. *J. Raman Spectrosc.* **2008**, *39*, 1396.
(25) Podstawka, E.; Kafarski, P.; Proniewicz, L. M. *J. Raman Spectrosc.* **2008**, *39*, in press. DOI: 10.1002/jrs.2000.
(26) Podstawka, E.; Ozaki, Y.; Proniewicz, L. M. *Langmuir* **2008**, *24*, 10807.
(27) Vargas, R.; Garza, J.; Hay, B. P.; Dixon, D. A. *J. Phys. Chem. A* **2002**, *106*, 3213.

(28) Ramankrishnan, C.; Paul, P. K. C.; Ramnarayan, K. *Proc. Int. Symp. Biomol. Struct, Interactions, Suppl. J. Biosci.* **1985**, *8*, 239.
(29) Anishetty, S.; Pennathur, G.; Anishetty, R. *BMC Struct. Biol.* **2002**, *2*, 9.
(30) Lejczak, B.; Kafarski, P.; Sztajer, H.; Mastalerz, P. *J. Med. Chem.* **1986**, *29*, 2211.
(31) Frisch, M. J. ; Trucks, G. W.; Schlegel, H. B.; Scuseria, G. E. Robb, M. A.; Cheeseman, J. R.; Zakrzewski, V. G.; Montgomery, J. A.; Stratmann, R. E.; Burant, J. C.; Dapprich, S.; Millam, J. M.; Daniels, A. D.; Kudin, K. N.; Strain, M. C.; Farkas, O.; Tomasi, J.; Barone, V.; Cossi, M.; Cammi, R.; Mennucci, B.; Pomelli, C.; Adamo, C.; Clifford, S.; Ochterski, J.; Petersson, G. A.; Ayala, P. Y.; Cui, Q.; Morokuma, K.; Malick, D. K.; Rabuck, A. D.; Raghavachari, K.; Foresman, J. B.; Cioslowski, J.; Ortiz, J. V.; Stefanov, B. B.; Liu, G. Liashenko, A.; Piskorz, P.; Komaromi, I.; Gomperts, R.; Martin, R. L.; Fox, D. J.; Keith, T.; Al-Laham, M. A.; Peng, C. Y.; Nanayakkara, A.; Gonzalez, C.; Challacombe, M.; Gill, P. M. W.; Johnson, B. G.; Chen, W.; Wong, M. W.; Andres, J. L.; Head-Gordon, M.; Replogle, E. S.; Pople, J. A. *Gaussian 98 (Revision A.1)*; Gaussian Inc.: Pittsburgh PA, 1998.
(32) Lee, C.; Yang, W.; Parr, R. G. *Phys. Rev.* **1988**, *B37*, 785.
(33) Becke, A. D. *J. Chem. Phys.* **1993**, *98*, 5648.
(34) O'Boyle. N. M.; Vos. J. G. GaussSum 0.8, Dublin City University, 2004. Available athttp://gausssum.sourceforge.net.
(35) Martin, J. M. L.; Van Alsenoy, C. *GAR2PED*; University of Antwerp, Antwerp, 1995.
(36) Podstawka, E.; Ozaki, Y.; Proniewicz, L. M. *Appl. Spectrosc.* **2004**, *58*, 580.
(37) Podstawka, E.; Ozaki, Y.; Proniewicz, L. M. *Appl. Spectrosc.* **2004**, *58*, 570.
(38) Lee, H. I.; Kim, M. S.; Suh, S. W. *Bull. Korean Chem. Soc.* **1998**, *9*, 218.
(39) Steward, S.; Fredericks, P. M. *Spectrochim. Acta, Part A* **1999**, *55*, 1641.
(40) Brolo, A. G.; Germain, P.; Hager, G. *J. Phys. Chem.* **2002**, *106*, 5982.
(41) Dakkouri, A. S.; Kolb, D. M.; Edelstein-Shima, R.; Mantler, D. *Langmuir* **1996**, *12*, 2849.
(42) Som, J. N.; Mukherjee, D. K. *J. Mol. Struct.* **1975**, *26*, 120.
(43) Mizushima, S.; Shimanouchi, T.; Nakamura, K.; Hayashi, M.; Tsuchiya, S. *J. Chem. Phys.* **1957**, *26*, 970.
(44) Nogami, N.; Sugeta, H.; Miyazawa, T. *Bull. Chem. Soc. Jpn.* **1975**, *48*, 2417.
(45) Nogami, N.; Sugeta, H.; Miyazawa, T. *Bull. Chem. Soc. Jpn.* **1975**, *48*, 3573.
(46) Suh, J. S.; Moskovits, M. *J. Am. Chem. Soc.* **1986**, *108*, 4711.
(47) Steward, S.; Fredericks, P. M. *Spectrochim. Acta, Part A* **1999**, *55*, 1641.
(48) Dou, X. M.; Ozaki, Y. *Rev. Anal. Chem.* **1999**, *18*, 285.
(49) Rava, R. P.; Spiro, T. G. *J. Phys. Chem.* **1985**, *89*, 1856.
(50) Asher, S. A.; Ludwig, M.; Johnson, C. R. *J. Am. Chem. Soc.* **1986**, *108*, 3186.
(51) Tu, A. T. *Advances in Spectroscopy: Spectroscopy of Biological Systems*; Clark, R. J. H., Hester R. E., Eds.; John Wiley and Sons: New York, 1986; Chapter 2, p 47.
(52) Podstawka, E. *Biopolymers* **2008**, *89*, 506.
(53) Greaves, S. J.; Griffith, P. *J. Raman Spectrosc.* **1988**, *19*, 503.
(54) Siiman, O.; Feilchenfeld, H. *J. Phys. Chem.* **1988**, *92*, 453.
(55) Dorain, P. B.; Von Raben, K. U.; Chang, R. K. *Surf. Sci.* **1984**, *148*, 439.
(56) Niaura, G.; Gaigalas, A. K.; Vilker, V. L. *J. Phys. Chem. B* **1997**, *101*, 9250.
(57) Chang, R. K. *Ber. Bunsen-Ges. Phys. Chem.* **1987**, *91*, 296.
(58) Gao, P.; Weaver, M. J. *J. Phys. Chem.* **1986**, *90*, 4057.
(59) Kim, S. K.; Kim, M. S.; Suh, S. W. *J. Raman Spectrosc.* **1987**, *18*, 171.

JP803674Q